Numerical and Experimental Studies on Electromagnetic Pulse Crimping of Joining D9 Steel Tube on SS316L (N) Plug

A. R. Dhiware[1*], S. D. Kore[2], M. R. Kulkarni[3]

[1]Lecturer, Department of Mechanical Engineering, Veermata Jijabai Technological Institute, Mumbai.
[2]Director, Veermata Jijabai Technological Institute, Mumbai.
[3]Accelerator and Pulse Power Division, Bhabha Atomic Research Centre, Mumbai.
*Corresponding author. Email: ardhiware@me.vjti.ac.in

Abstract

Electromagnetic Pulse crimping process is an advanced technique that utilises high-intensity electromagnetic forces to deform and join metallic components. This study investigates numerical simulations and experimental work on the EM crimping process used to crimp the D9 steel tube to SS316L (N) plug. Optimum values of tube impact velocity and displacement at the D9 steel tube with SS316L (N) plug are determined using COMSOL© Multiphysics simulations. Effects of process parameters such as current, magnetic field, plastic strain, impact velocity and voltage levels are investigated for their effect on crimping of D9 tube.
In an EM Pulse crimping process experimental RLC setup was used for producing the excitation current. Experiments are performed for different discharge voltages for D9 steel tube, SS316L (N) plug, copper driver and field shaper setup. The metallurgical characterisation was performed using optical microscopy to check the weld line for bonding. The experimental and simulation data show good agreement for the deformation of the D9 tube. As voltage or energy input increases, keeping RLC constant, an increase in impact velocity, effective plastic strain, deformation, and peak coil current is observed. At the same time, the frequency of the current remains constant, which is favourable for EM Pulse crimping.

Keywords

Electromagnetic Pulse crimping, Impact Velocity, Magnetic Flux density, Voltage.

1 Introduction

EM Pulse crimping is an advanced, high strain rate metal joining technique that utilizes Lorentz forces to achieve deformation and bonding without direct mechanical contact. It can be applied to sheet metal, tube-to-tube, or tube-to-bar joining configurations. In fast breeder, D9 tubes are used for fuel cladding and SS316L (N) plugs used for sealing or capping these tubes during fabrication or assembly. (Rajak & Kore, 2017) reported that EM pulse crimping is an advantageous process for joining dissimilar metals with different mechanical properties. (Psyk et al., 2011) research focuses on working principles of EM forming, deformation pattern of workpiece and flow of energy. Kumar et al (2020) demonstrated the EM pulse welding of steel to steel in combination with microscopic examination.(Shen et al., 2022)reported that EM pulse crimping is a promising method for connecting high-voltage wiring in electric vehicles. Experiments on aluminium tubes showed that optimal crimping occurs when the size of the field-shaper is shorter than that of EM coil, and their gaps form a 90° angle.

This paper presents a numerical simulation of joining a D9 tube to an SS316L (N) plug using EM Pulse Crimping with a single-taper field shaper, compared to experimental results. The authors validated the experimental results with numerical analysis and examined the effects of process parameters, such as current, magnetic field, plastic strain, impact velocity and deformation at different voltages.

2 EM pulse crimping setup

Fig.1 illustrates the EM configuration employed in the EM crimping process. Upon closing the circuit switch, the energy accumulated in the capacitor is released. The crimping coil's fluctuating magnetic field produces magnetic pressure.

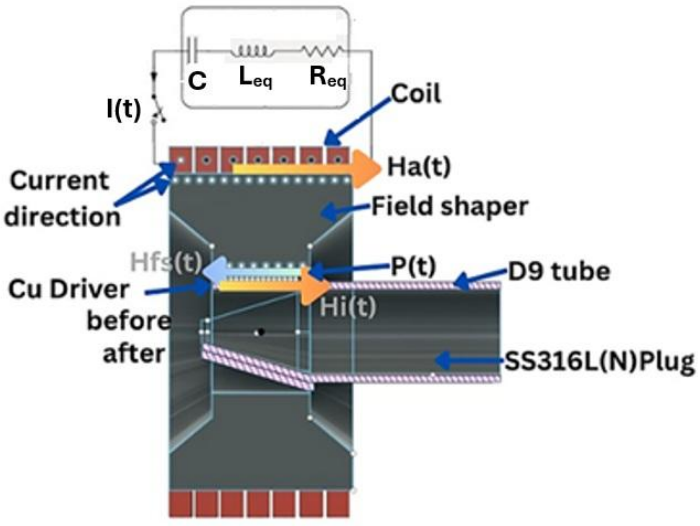

***Figure 1**: EM pulse crimping setup*

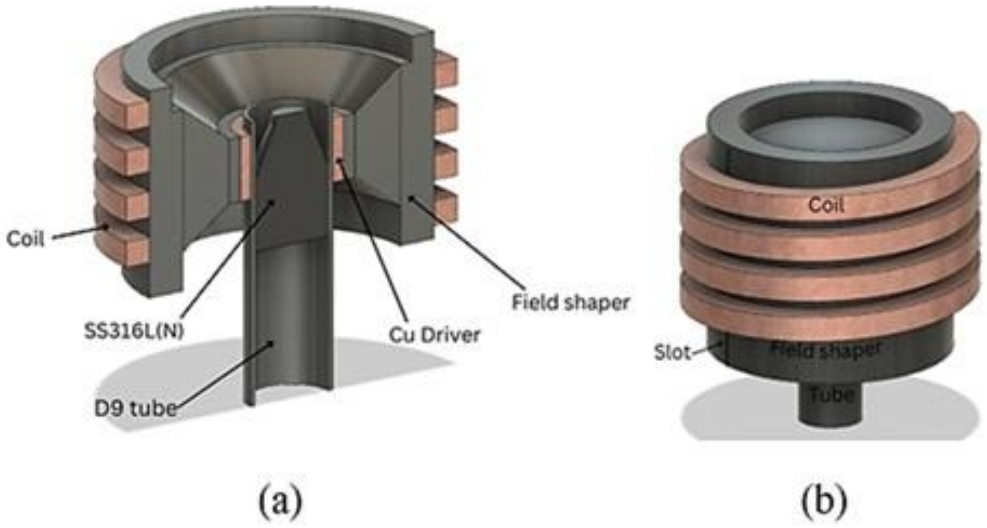

Figure 2: *Components of EM crimping*

The coaxially aligned D9 tube and SS316L(N) plug are crimped by a Cu driver, which is accelerated by Lorentz force generated from eddy currents induced by the coil's magnetic field, pushing the workpiece beyond its yield strength. The EM equipment, rated at 40 kJ, operates with a charging voltage of 20 kV and a capacitance of 224 μF. It functions at a frequency of 16 kHz and produces a peak current of 450 kA at 20 kV. Fig.2 (a) shows the schematic diagram of the components of the EM crimping process.

2.1 Coil, Field-shaper and Workpiece

The 4-turn copper coil (Fig. 2 b) generates the magnetic field and pressure for EM forming. Its first and last turns measure 65×12 mm, the middle turns 65×16 mm, with an inner diameter of 90 mm and outer diameter of 220 mm. The field shaper employed is a tapered copper type with an axial slit measuring 0.8 mm, The field shaper is utilized to focus the magnetic field on the critical area of the workpiece to achieve a mechanical joint between the D9 steel tube and the SS316L(N) plug. The D9 steel tube and SS316L(N) plug combination with copper driver is used as a workpiece in this work. The coil is kept over the workpiece. The D9 steel tubular structure is crimped to the SS316L (N) plug in this study.

3 Numerical simulation using COMSOL© Multiphysics

The simulation uses the AC/DC module to solve Maxwell’s equations for magnetic fields. An RLC circuit charges a capacitor, which discharges through a trigger switch to generate current in the coil. The flyer tube is placed in proximity to the EM coil, which induces current in flyer tube, **Eq. 1** gives the value of discharging energy (E), and Eq. 2 provides the value of charging voltage (V) in terms of capacitance (C) and inductance(L) and current (I).

$$E = \frac{1}{2}CV^2 \tag{1}$$

$$V = \frac{I}{\sqrt{\frac{C}{L}}} \tag{2}$$

This system uses Maxwell's equation.

$$\frac{d^2I(t)}{dt^2} + 2\xi\omega\frac{dI(t)}{dt} + \omega^2 I(t) = 0 \tag{3}$$

By solving differential Eq. 3, the resultant coil currents I in Eq. 4 are obtained, representing a damped sinusoidal wave with initial discharge voltage V, damping factor β, and angular frequency ω, and Time t.

$$I(t) = \frac{V}{L\omega}e^{(-\beta t)}\,sin(\,\omega t) \tag{4}$$

The magnetic pressure and the Lorentz force are generated from the discharging current. The magnetic force acts on the D9 tube and the formula for calculating the Lorenz force (f) involves current density (J) and magnetic flux density (B) as per Eq. 5. The magnetic flux density norm B (t) and magnetic field strength intensity H (t) are provided by Eq. 6 and 7.

$$f = J \times \mathrm{B} = \frac{1}{\mu}(\nabla \times B) \times \mathrm{B} \tag{5}$$

$$B(t) = \mu\frac{N}{l}I(t) \tag{6}$$

$$H(t) = \frac{NI(t)}{l} \tag{7}$$

In this context, N represents the number of turns in the EM coil, l denotes the coil's length, and μ stands for the magnetic permeability of the coil's material. This gives output as magnetic fields, meaning Lorentz forces are produced. The result of the EM module is given as input to the solid mechanics module, which produces deformation. Figure 3 shows this Multiphysics simulation process. The Cowper-Symonds constitutive model in Eq. 8, as reported by (Kapil & Sharma, 2015) It is used to find out the plastic deformation of the workpiece at each time increment.

$$\sigma = \sigma_y \left[1 + \left(\frac{\dot{\varepsilon}}{p}\right)^m\right] \quad (8)$$

Here, σ_y = flow stress, p and m = specific material constants and $\dot{\varepsilon}$ = plastic strain rate (s^{-1}). In COMSOL© Multiphysics, this Cower-Symonds constitutive model is a swift option in the solid mechanic's module.

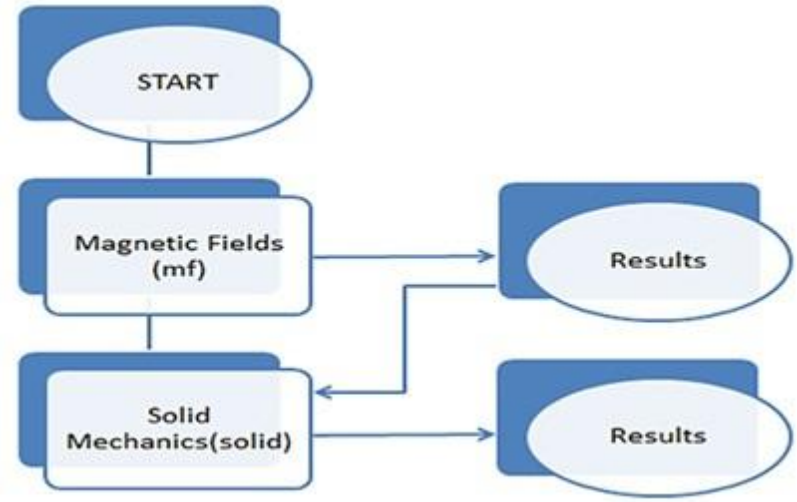

***Figure 3**: Flowchart of coupled simulation*

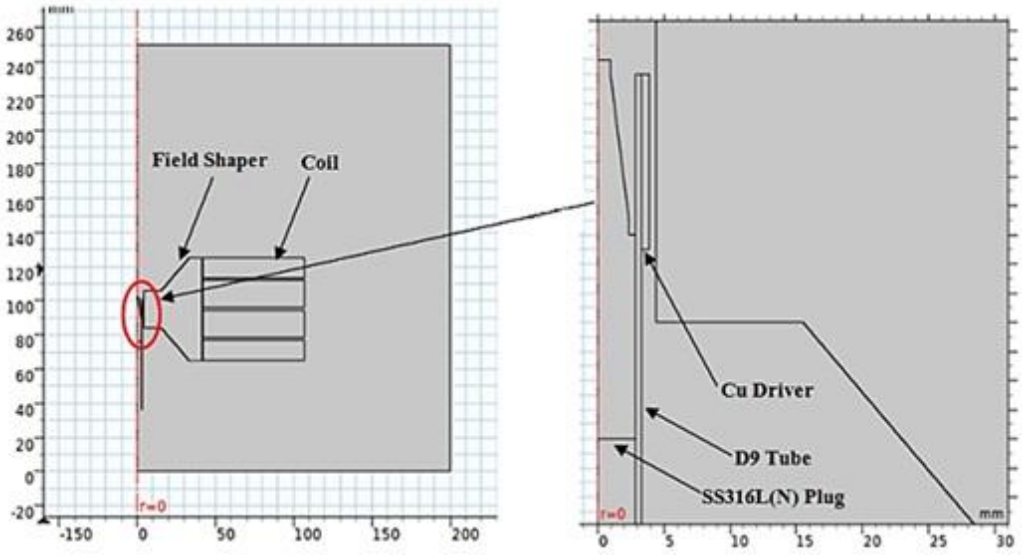

***Figure 4**: 2D axisymmetric model*

Fig. 4 shows the 2D axisymmetric model of EM crimping, with a coaxial copper coil, D9 tube, Cu driver, and SS316L(N) plug. Only half the setup is modelled due to symmetry. Simulation inputs, including RLC values, are listed in **Table** 1.

Charging voltage (kV)	15	16	17	18
Current frequency (kHz)	16			
Inductance (μH)	1.8			
Capacitance (μF)	224			
Resistance (mΩ)	9.38			
Angular Frequency (rad/s)	100530.96			

***Table 1**: Process Parameters*

Voltage	Peak Coil Current (kA)	
	Experimental Values	Simulation Values
15kV	310	299.77
16kV	334	338.87
17kV	354	352.17
18kV	374	375.16

***Table 2:** Peak Coil Current (kA)*

4 Results and Discussion

4.1 Current Curve

Fig. 5 and Fig. 6 illustrate the current waveform in the EM Crimping process, comparing experimental and 15kV, 16kV, 17kV, and 18kV simulation results. The current is measured using rogowski coil as reported by (Nadimetla et al., 2024) as shown in Fig. 5 as an experimental curve. Table 2 summarizes the Peak coil current values obtained in experimental and simulation during the EM Crimping process at discharge voltages.

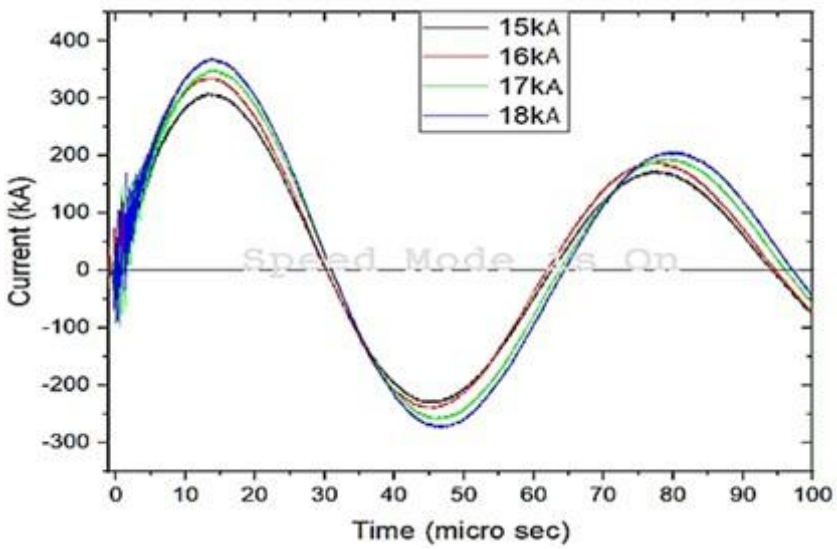

***Figure 5** Experimental curve of Time Vs coil current for 15kV, 16kV, 17kV, and 18kV*

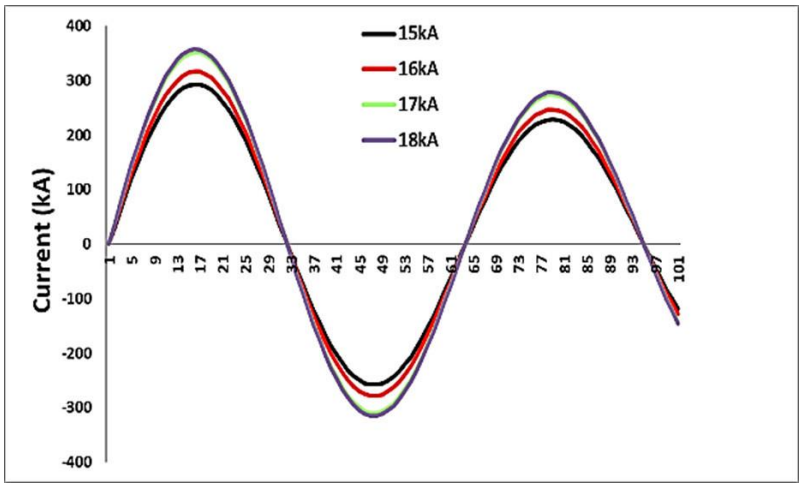

Figure 6 *Simulation curve of Time Vs coil current for 15kV, 16kV, 17kV, and 18kV*

4.2 Displacement

Experiments and simulations at 15–18 kV (Fig. 7 a–d) show non-uniform deformation along the D9 tube due to uneven magnetic pressure. Simulation results closely match experimental data, with 98% accuracy. The strong correlation confirms the reliability of numerical methods for predicting EM behaviour, though minor local deviations may result from material variations, mesh resolution, or experimental misalignments. Fig. 8 shows rapid, localised displacement at 15 kV, with peak deformation at all three tube locations occurring within microseconds.

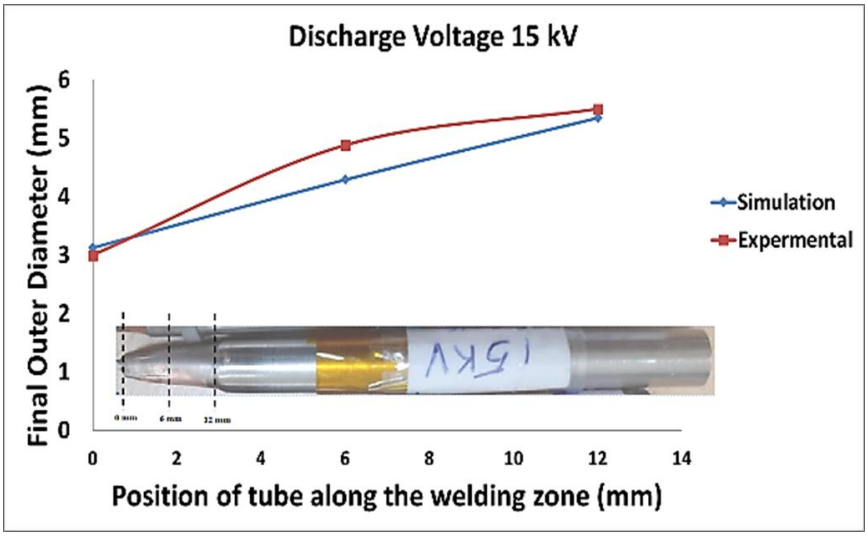

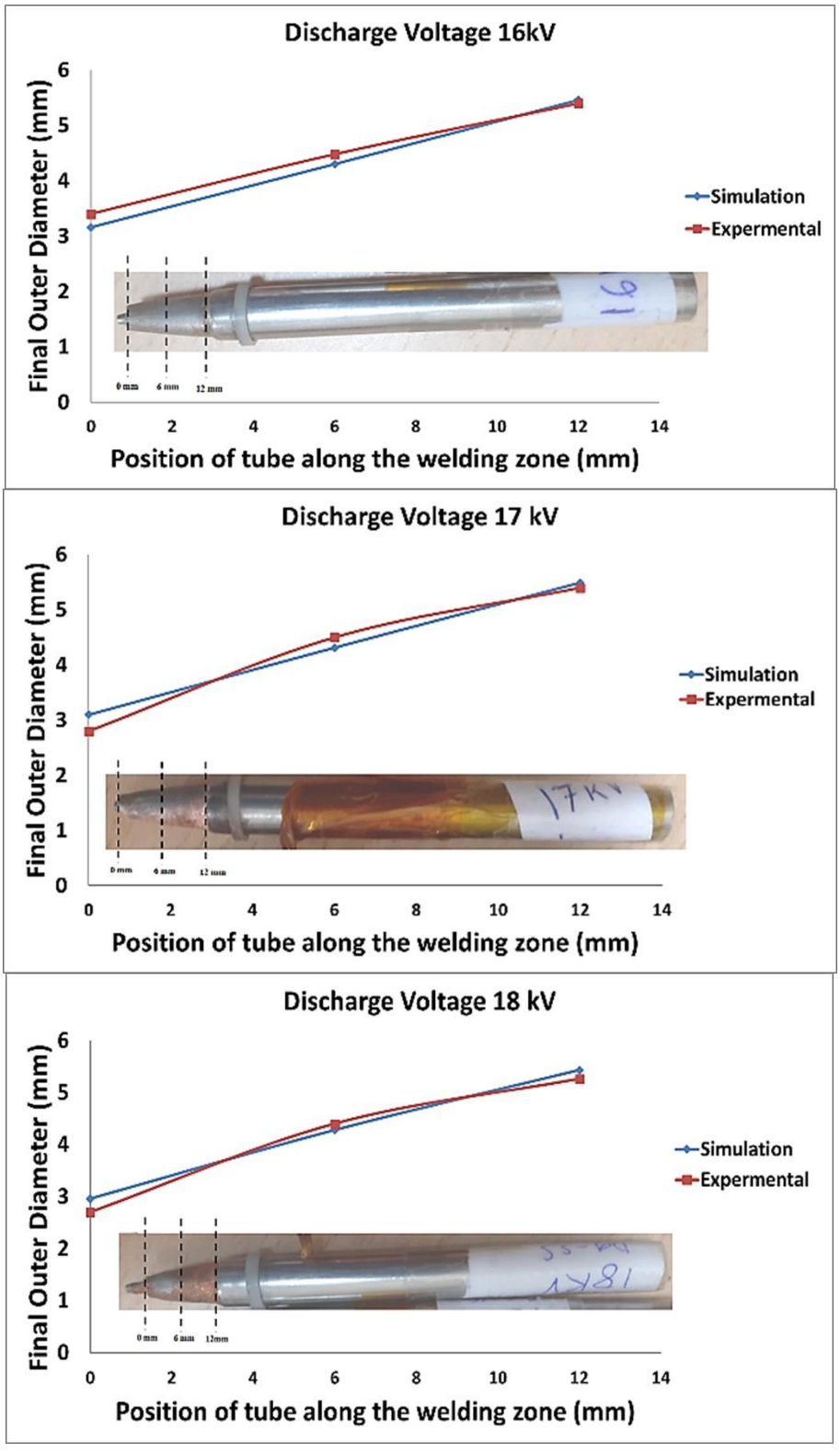

Figure 7. Outer diameter deformation of D9 Tube for (a)15 kV discharge, (b) 16 kV discharge, (c) 17 kV discharge, (d) 18 kV discharge.

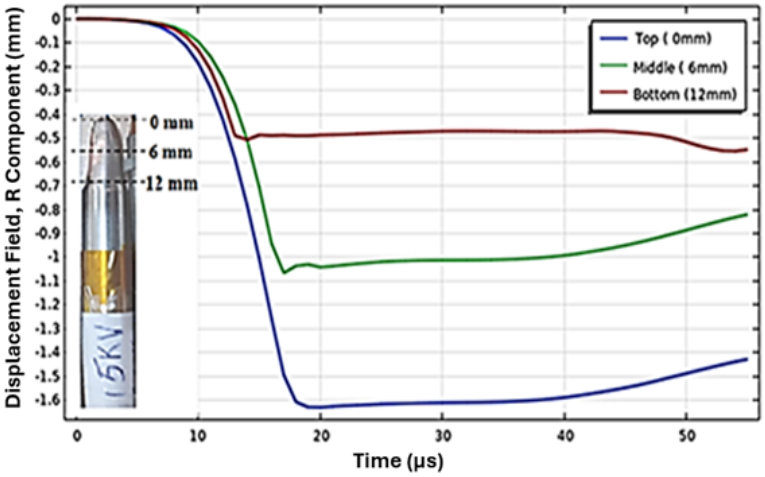

Figure 8: *Time Vs the radial Displacement*

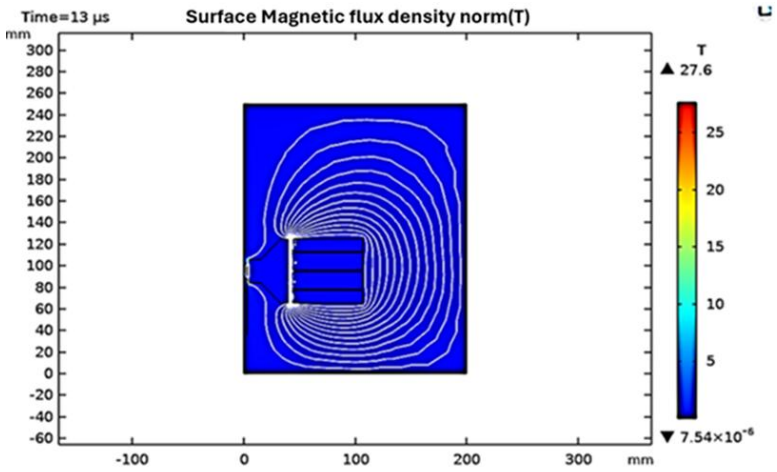

Figure 9: *Magnetic field of a complete system*

The findings validate the model and highlight how discharge voltage affects deformation. Peak electromagnetic force causes rapid initial acceleration and a sharp rise in radial displacement. After 18 µs, the EM force drops as the current decays. Around 40 µs, a secondary pulse induces a weaker force, causing slight oscillations in radial displacement due to inertia and internal stresses.

4.3 Magnetic Field

Each turn of the EM coil generates a localized magnetic field, which collectively results in a concentrated field at the top portion of the D9 tube, as illustrated in Fig. 9. This is due to the superimposed effect of the coil turns, leading to higher field intensity near the starting turn region. The simulation results presented in Fig. 10 show that the maximum magnetic

field varies significantly along the outer wall of the field shaper Points A and C are positioned adjacent to coil turns, whereas Point B is located next to the gap between two coil turns: point A (top end) exhibits 23 T, point B (middle) 14 T, and point C (bottom end) 22 T. This non-uniformity confirms that the EM force acting on the tube is position-dependent, influencing the localized deformation observed experimentally. Fig. 11 further shows that the highest magnetic flux densities are achieved between the inner wall of the field shaper and the copper driver, reaching 40T at points A and C and 39T at point B. The analysis is strengthened by detailed magnetic field mapping at key points, explaining the observed asymmetrical deformation. Though based on ideal coil symmetry and uniform material, the model closely matches experimental results, indicating it effectively captures the core process physics.

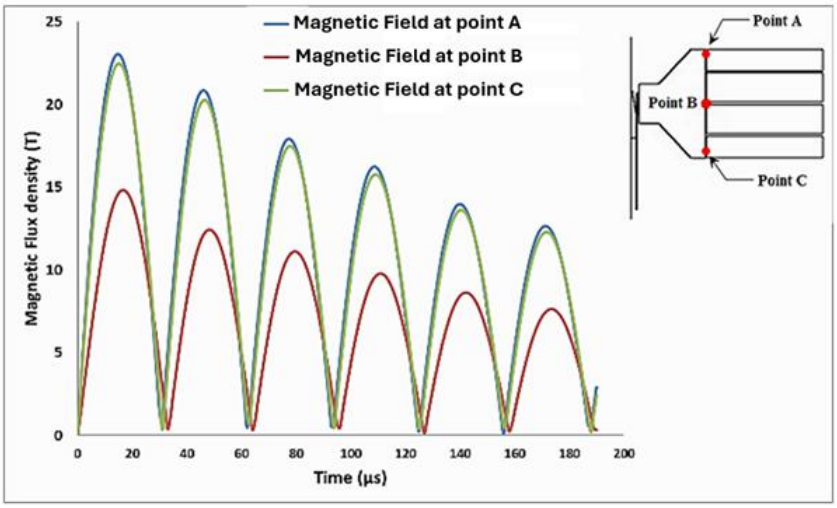

***Figure 10**: Time Vs. Magnetic Field at the gap between the coil & the field shaper (input voltage -15kV)*

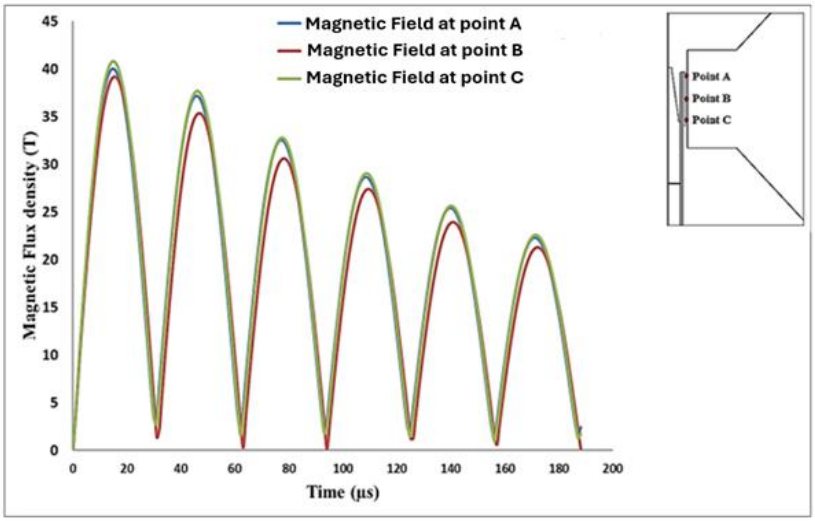

***Figure 11**: Time Vs Magnetic Field at the gap between Cu driver & field shaper (input voltage -15 kV)*

4.4 Impact Velocity

Impact velocity plays a critical role in the effectiveness and outcome of EM, as it directly influences the strain rate and degree of plastic deformation in the workpiece. Fig. 12 presents the impact velocity at three cut sections—points A, B, and C—along the length of the D9 tube at a discharge voltage of 15 kV. At point A (top end), the peak impact velocity reaches 287.07 m/s at 15 µs. At point B (middle), it is 203.50 m/s at 14 µs, and at point C (bottom end), it is 147.98 m/s at 13 µs. Impact velocity decreases from the tube top to bottom, matching the non-uniform magnetic field. Higher top velocity improves formability but risks defects, while lower bottom velocity may cause incomplete forming. Despite minor assumptions, velocity trends closely match experiments, validating the simulation.

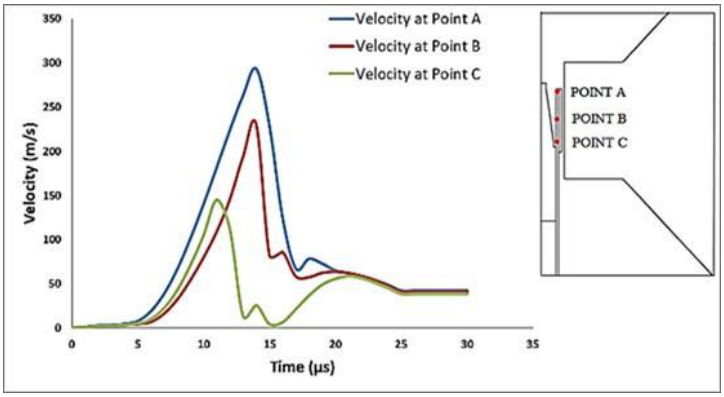

***Figure 12**: Time Vs velocity of the tube (input voltage-15 kV)*

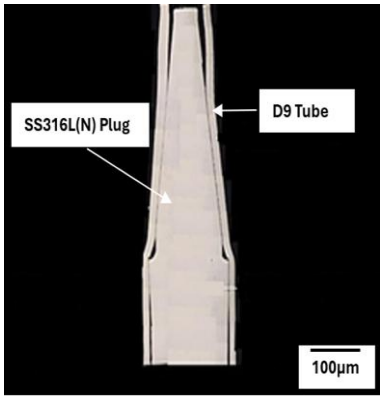

***Figure 13**: Optical micrograph of EM crimping sample*

4.5 Characterization of the crimped samples

Joint quality is first evaluated visually for shape and geometry. Crimped microsections are prepared by abrasive wet cutting with an Al_2O_3 wheel, followed by hot mounting. Polishing is done using 200–1000 grit SiC papers and Al_2O_3 suspensions (5 µm and 1.5 µm), then etched for 3 minutes in a nitric-hydrofluoric acid solution.

Optical microscopy (Fig.13) shows no metallurgical bonding in the EM crimped joint between the D9 tube and SS316L(N) plug. Joints form mainly by mechanical interlocking through plastic deformation, suitable for many structural uses but less so for hermetic sealing or high loads. This analysis confirms the joining mechanism with microstructural evidence.

4.6 Effect of voltage on EM crimping

Fig. 14 to 16 collectively highlight the influence of discharge voltage on key EM parameters, namely, magnetic field strength, impact velocity and effective plastic strain of the workpiece. Fig. 14 shows that peak magnetic field strength rises with discharge voltage, driving stronger EM forces. This aligns with the initial velocity rise in Fig. 15, confirming their causal link Fig. 15 shows workpiece velocity rising with discharge voltage, peaking at 293.59 m/s at 18 kV, due to stronger EM forces and magnetic pressure, consistent with EMF principles.

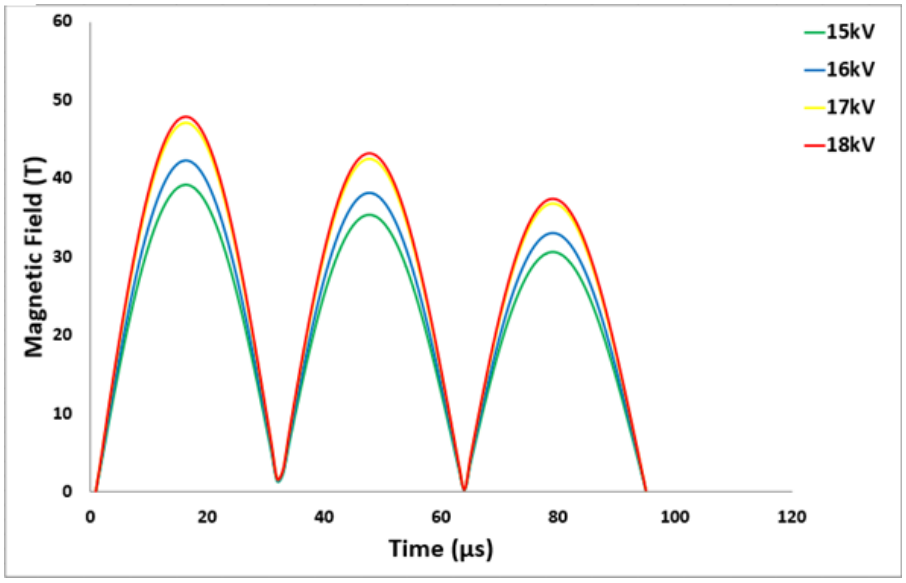

***Figure 14**: Variation in magnetic field density norm with time at different discharge voltages*

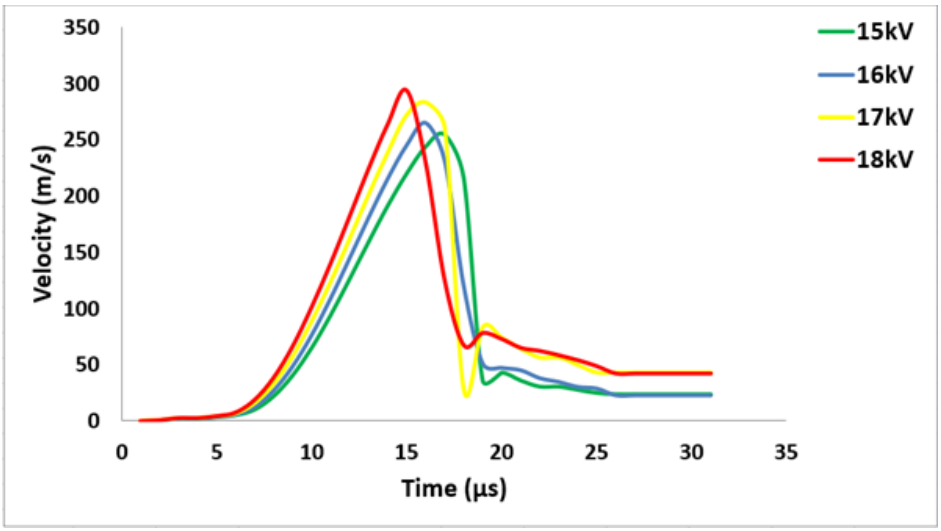

***Figure 15**: Variation in impact velocity with time at different discharge voltages.*

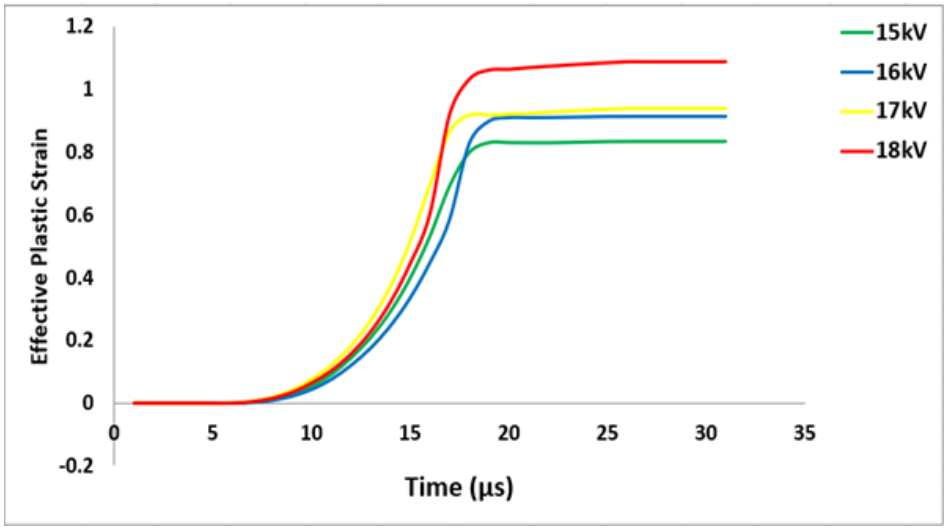

***Figure 16**: Variation in effective plastic strain with time at different discharge voltages*

Fig. 16 illustrates how this enhanced dynamic loading influences material deformation. The effective plastic strain of the workpiece increases with discharge voltage, peaking at 1.0309 at 18 kV. Higher EM force boosts forming velocity and deformation, increasing plastic strain and energy absorption. This helps complex forming but requires careful voltage control to avoid material failure, highlighting the need to optimize discharge voltage.

5 Conclusions

In the present study, Numerical Simulation of joining of D9Tube to SS316L (N) Plug by EM Pulse Crimping with Field Shaper is carried out compared with the experimental work, and the following are the conclusions from this study:

- Though experiments used a 4-turn coil with peak displacement at the tube top and 40 T field at the field shaper center, the results apply to similar coil setups, as the field shaper critically amplifies magnetic intensity in the forming zone.
- The radial displacement graph from the 2D-axisymmetric COMSOL© Multiphysics simulation shows strong agreement (98%) with experimental results.
- The optical micrograph reveals a mechanical fit with no evidence of metallurgical bonding.
- With increased voltage or energy input while keeping resistance (R), inductance (L), and capacitance (C) constant, impact velocity, effective plastic strain, deformation, peak coil current, and stress all increase, whereas the current frequency remains unchanged. This behaviour is favourable for EM crimping.

References

Kapil, A., & Sharma, A. (2015). Coupled Electromagnetic–Structural Simulation of Magnetic Pulse Welding. In *Topics in Mining, Metallurgy and Materials Engineering* (pp. 255–272). Springer Science and Business Media Deutschland GmbH. https://doi.org/10.1007/978-81-322-2355-9_13

Nadimetla, T., Kumar, L., Kumar, R., Kulkarni, M. R., & Kore, S. D. (2024). Experimental Investigation and Metallurgical Studies on D9 Tube to SS316 Tapered End Plug Using Magnetic Pulse Welding. *Journal of Materials Engineering and Performance*. https://doi.org/10.1007/s11665-024-10029-0

Psyk, V., Risch, D., Kinsey, B. L., Tekkaya, A. E., & Kleiner, M. (2011). Electromagnetic forming - A review. *Journal of Materials Processing Technology*, *211*(5), 787–829. https://doi.org/10.1016/j.jmatprotec.2010.12.012

Rajak, A. K., & Kore, S. D. (2017). Experimental investigation of aluminium–copper wire crimping with electromagnetic process: Its advantages over conventional process. *Journal of Manufacturing Processes*, *26*, 57–66. https://doi.org/10.1016/j.jmapro.2017.01.009

Shen, T., Li, C., Zhou, Y., Wu, H., Wang, X., & Xu, Q. (2022). The effect of assembly of coil and field shaper on electromagnetic pulse crimping. *Energy Reports*, *8*, 1243–1248. https://doi.org/10.1016/j.egyr.2021.11.213